

## The impact of surface-wave attenuation on 3-D seismic survey design

Ishiyama, Tomohide; Blacquièrè, Gerrit; Mulder, Wim A.

**DOI**

[10.1111/1365-2478.12370](https://doi.org/10.1111/1365-2478.12370)

**Publication date**

2017

**Document Version**

Final published version

**Published in**

Geophysical Prospecting

**Citation (APA)**

Ishiyama, T., Blacquièrè, G., & Mulder, W. A. (2017). The impact of surface-wave attenuation on 3-D seismic survey design. *Geophysical Prospecting*, *65*(1), 86-96. <https://doi.org/10.1111/1365-2478.12370>

**Important note**

To cite this publication, please use the final published version (if applicable). Please check the document version above.

**Copyright**

Other than for strictly personal use, it is not permitted to download, forward or distribute the text or part of it, without the consent of the author(s) and/or copyright holder(s), unless the work is under an open content license such as Creative Commons.

**Takedown policy**

Please contact us and provide details if you believe this document breaches copyrights. We will remove access to the work immediately and investigate your claim.

# The impact of surface-wave attenuation on 3-D seismic survey design

Tomohide Ishiyama<sup>1,2\*</sup>, Gerrit Blacquière<sup>1</sup> and Wim A. Mulder<sup>1,3</sup>

<sup>1</sup>Department of Geotechnology, Faculty of Civil Engineering and Geosciences, Delft University of Technology, PO Box 5048, 2600 GA Delft, The Netherlands, <sup>2</sup>Inpex Corporation, 5-3-1 Akasaka, Minato-ku, Tokyo 107-6332, Japan, and <sup>3</sup>Shell Global Solutions International B.V., Kessler Park 1, 2288 GS Rijswijk, The Netherlands

Received September 2014, revision accepted January 2016

## ABSTRACT

Three-dimensional seismic survey design should provide an acquisition geometry that enables imaging and amplitude-versus-offset applications of target reflectors with sufficient data quality under given economical and operational constraints. However, in land or shallow-water environments, surface waves are often dominant in the seismic data. The effectiveness of surface-wave separation or attenuation significantly affects the quality of the final result. Therefore, the need for surface-wave attenuation imposes additional constraints on the acquisition geometry. Recently, we have proposed a method for surface-wave attenuation that can better deal with aliased seismic data than classic methods such as slowness/velocity-based filtering. Here, we investigate how surface-wave attenuation affects the selection of survey parameters and the resulting data quality. To quantify the latter, we introduce a measure that represents the estimated signal-to-noise ratio between the desired subsurface signal and the surface waves that are deemed to be noise. In a case study, we applied surface-wave attenuation and signal-to-noise ratio estimation to several data sets with different survey parameters. The spatial sampling intervals of the basic subset are the survey parameters that affect the performance of surface-wave attenuation methods the most. Finer spatial sampling will reduce aliasing and make surface-wave attenuation easier, resulting in better data quality until no further improvement is obtained. We observed this behaviour as a main trend that levels off at increasingly denser sampling. With our method, this trend curve lies at a considerably higher signal-to-noise ratio than with a classic filtering method. This means that we can obtain a much better data quality for given survey effort or the same data quality as with a conventional method at a lower cost.

**Key words:** Survey design, Parameter estimation, Surface wave, Noise attenuation, Signal-to-noise ratio.

## INTRODUCTION

For 3-D seismic surveys, one should choose the survey parameters such that the acquired data have the quality required to achieve the desired objectives. To obtain high data quality while reducing survey effort, several authors presented sophisticated approaches to survey design and evaluation. Traditionally, survey design is based on attributes such as fold,

offset, azimuth sampling in each bin, as well as their distribution across bins (e.g., Cordsen, Galbraith, and Peirce (2000); Galbraith (2004); and Vermeer (2012)). This approach provides the information from a given acquisition geometry at the surface but does not take into account subsurface structures and properties. More recent survey design methods involve the reconstruction of the angle-dependent reflectivity in one or more subsurface points in the target area (e.g., Berkhout *et al.* (2001); Volker *et al.* (2001); van Veldhuizen, Blacquière, and Berkhout (2008); and Ishiyama and Blacquière (2015)). In

\*E-mail: tomohide.ishiyama@inpex.co.jp

this way, survey design examines the capability of an acquisition geometry to properly image target reflectors and to allow for amplitude-versus-offset (AVO) analysis of the reflections.

Surface waves in land or shallow-water environments often mask the primary reflections. Therefore, they impose additional requirements on the acquisition geometry since it should allow for effective surface-wave separation or attenuation (Berteussen, Zhang, and Sun 2011). Many methods for surface-wave attenuation have been developed. Examples are conventional filtering methods (e.g., Yilmaz (2001)) and a data-driven, data-adaptive, and model-based method using a closed-loop approach (Ishiyama *et al.* (2015)). These approaches remove the estimated surface waves from the seismic data, although some residual may still be present in the result. To quantitatively analyse the data quality of the result, signal-to-noise ratio (SNR) can be used as a proper attribute or measure representing the data quality in terms of surface-wave attenuation. The residual affects the effectiveness of subsequent stages of data processing, imaging, and, ultimately, reservoir characterization and may consequently adversely influence the final product. Therefore, the effectiveness of surface-wave attenuation for a given acquisition geometry will have an impact on survey design.

For 3-D seismic surveys, the basic survey parameters are the four spatial sampling intervals and apertures of the template geometry (Vermeer, 2012). The four spatial sampling intervals are defined by the receiver and source intervals, each in two sampling directions that are usually orthogonal. The four spatial sampling apertures consist in the receiver and source apertures, oriented in the same way as the above four spatial coordinates. Given these survey parameters, we will address the following questions.

- (i) What is the relationship between the survey parameters and the resulting data quality?
- (ii) Which types of survey parameters are essential?
- (iii) What are the optimal values of the key types of survey parameters for the required data quality?
- (iv) How does the method of surface-wave attenuation affect these values?

To answer these questions, we applied surface-wave attenuation and SNR estimation to several data sets with different survey parameters and analysed the relationship between the survey parameters and the resulting data quality. We considered two methods for surface-wave attenuation, i.e., a conventional filtering method in the wavenumber–frequency ( $k_x k_y$ - $f$ ) domain and our new method using a closed-loop approach.

## METHOD

### Survey parameters and survey effort

As mentioned before, for 3-D seismic surveys, the relevant survey parameters are the spatial sampling intervals for receivers,  $\Delta x_d$  and  $\Delta y_d$ , and for sources,  $\Delta x_s$  and  $\Delta y_s$ , as well as their respective apertures, i.e.,  $X_d$  and  $Y_d$  for the receivers and  $X_s$  and  $Y_s$  for the sources in the template geometry. For an orthogonal geometry, the basic subset is a cross-spread gather, where receiver–point and source–point intervals are quite fine (for example,  $\Delta x_d$  and  $\Delta y_s$ ), whereas receiver–line and source–line intervals are often coarse ( $\Delta y_d$  and  $\Delta x_s$  in this example). Receiver–line and source–line lengths specify the maximum apertures ( $X_d$  and  $Y_s$  for this basic subset). For an areal geometry, the basic subset is a common-source gather or a common-receiver gather, where receivers are arranged on a densely spaced grid ( $\Delta x_d$  and  $\Delta y_d$  fine) and sources are arranged on a sparsely spaced grid ( $\Delta x_s$  and  $\Delta y_s$  coarse) or the other way around. Receiver-spread widths ( $X_d$  and  $Y_d$ ) and source-spread widths ( $X_s$  and  $Y_s$ ) specify the maximum apertures in the former and the latter cases, respectively. Two of the four spatial coordinates, represented by the set  $\{\Delta x_b, \Delta y_b, X_b, Y_b\}$ , specify the spatial sampling of the basic subset, where subscript  $b$  can be  $d$  or  $s$ , independently for each choice of survey parameters but not in arbitrary combinations. Two other coordinates, described by the set  $\{\Delta x_B, \Delta y_B\}$ , specify the spatial redundancy of the basic subsets, i.e., the fold, where again subscript  $B$  can be  $d$  or  $s$ . Their maximum apertures,  $X_B$  and  $Y_B$ , are usually the same as  $X_b$  and  $Y_b$  and define the template. For instance, the set  $\{\Delta x_d, \Delta y_s, X_d, Y_s\}$  specifies the spatial sampling of a cross-spread gather, i.e.,  $\{\Delta x_b, \Delta y_b, X_b, Y_b\} = \{\Delta x_d, \Delta y_s, X_d, Y_s\}$ , whereas the set  $\{\Delta x_s, \Delta y_d\}$  specifies the spatial redundancy of the cross-spread gather, i.e.,  $\{\Delta x_B, \Delta y_B\} = \{\Delta x_s, \Delta y_d\}$ . Here, the  $x$ -direction is considered as the in-line direction.

Surface-wave attenuation is often applied to basic subsets such as 3-D common-shot, 3-D common-receiver, and 3-D cross-spread gathers. Therefore, the key set of survey parameters in terms of the surface-wave attenuation is  $\{\Delta x_b, \Delta y_b, X_b, Y_b\}$ , specifying the spatial sampling of the basic subset. Consequently, we can define the survey effort,  $SE$ , as a combined attribute of these survey parameters relative to a reference basic subset as

$$SE = \frac{\Delta x_{bref}}{\Delta x_b} \frac{\Delta y_{bref}}{\Delta y_b} \frac{X_b}{X_{bref}} \frac{Y_b}{Y_{bref}}, \quad (1)$$

where subscript “ref” denotes “reference”. We also define two attributes that measure symmetry

$$A_{\Delta x_b} = \frac{\Delta x_b}{\Delta y_b}, \quad (2)$$

$$A_{X_b} = \frac{Y_b}{X_b}, \quad (3)$$

where  $A_{\Delta x_b}$  is the aspect ratio of the spatial sampling intervals, and  $A_{X_b}$  is the aspect ratio of the spatial sampling apertures.

### Surface-wave attenuation

We considered two methods for surface-wave attenuation. For the description of these methods, we adopt the representation of a 3-D seismic data set as a matrix for each monochromatic component (Berkhout, 1982). In this matrix, column vectors correspond to common-source gathers and row vectors constitute common-receiver gathers. Using reciprocity, a common-receiver gather can be thought of as a common-source gather. Cross-spread gathers can be rearranged into common-source gathers by sorting the cross-spread gathers into the corresponding vectors by lexicographical ordering. Since the discrete Fourier transform is invertible, either of the space–frequency ( $xy$ - $f$ ) or the space–time ( $xy$ - $t$ ) domain can be used, depending on what is most convenient or efficient. In the matrix representation, a common-source gather containing both subsurface signals and surface waves can be written as  $(\vec{P} + \vec{N})$ , where  $\vec{P}$  represents the subsurface signals and  $\vec{N}$  represents the surface waves. Note that, in this paper, the term “subsurface signals” refers to all events except the surface waves, i.e.,  $\vec{P}$  includes refractions, reflections, surface-related and internal multiples, etc. In fact,  $\vec{P}$  contains not only the desired signal but also non-source-related noise such as ambient noise. If the surface waves  $\vec{N}$  are estimated and subtracted from the seismic data  $(\vec{P} + \vec{N})$ , we obtain the estimated subsurface signals  $\hat{\vec{P}}$ . Here, the hat symbol  $\hat{\cdot}$  denotes “estimated”. If  $\vec{N}$  is not perfectly estimated, a non-zero residual,  $\Delta\vec{N} = \vec{N} - \hat{\vec{N}}$ , remains. In that case,  $\hat{\vec{P}}$  includes the term  $\Delta\vec{N}$ , i.e.,  $\hat{\vec{P}} = (\vec{P} + \vec{N}) - \hat{\vec{N}} = \vec{P} + \Delta\vec{N}$ .

The first method is a conventional slowness/velocity-based filtering, in which  $(\vec{P} + \vec{N})$  is transformed to a suitable domain, e.g., the Radon ( $p_x p_y$ - $f$ ) or the  $k_x k_y$ - $f$  domain, where  $\vec{N}$  and  $\vec{P}$  are separated in terms of their apparent slowness/velocity. The conventional method generally has the limitation that  $\vec{N}$  does not fully contain the aliased energy and part of the aliased energy leaks into  $\hat{\vec{P}}$ .

The second method is our recently developed closed-loop or iterative approach (Ishiyama *et al.* (2015)). It employs

a relatively simple forward model of surface waves together with adaptive subtraction of the forward-modelled surface waves from the observed seismic data. The model is parameterized by frequency-dependent slowness and source properties for each surface-wave mode. The iterative scheme minimizes the residual or the difference between the observed and the modelled surface waves. This approach solves the inverse problem and, consequently, produces optimal  $\vec{N}$  and  $\hat{\vec{P}}$ , although  $\Delta\vec{N}$  that cannot be explained by the model may still remain.

An attractive property of our method is that it can be applied to undersampled, irregularly sampled, and blended seismic data. This offers the possibility of relaxing the requirements on the spatial sampling intervals and therefore offers flexibility with respect to the acquisition geometry. Figure 1 shows an example of our method using 3-D ocean-bottom-cable (OBC) hydrophone data acquired offshore Abu Dhabi in a shallow-water environment. We consider a cross-spread gather, consisting of a receiver line in the  $x$ -direction and a source line in the  $y$ -direction, each with a spatial sampling interval of 50 m and a length of 3200 m, i.e.,  $\{\Delta x_b, \Delta y_b, X_b, Y_b\} = \{50 \text{ m}, 50 \text{ m}, 3200 \text{ m}, 3200 \text{ m}\}$ ,  $A_{\Delta x_b} = 1$ , and  $A_{X_b} = 1$ . This fills a 3-D cube in the  $xy$ - $t$  domain. Bad traces were removed. Figures 1(a) and 1(d) exhibit  $(\vec{P} + \vec{N})$  in the  $xy$ - $t$  and the  $k_x k_y$ - $f$  domains, respectively. The surface waves distinguish themselves from the subsurface signals by larger amplitudes and lower frequencies. We can identify the fundamental mode and one higher mode. Each is shaped as a cone in the  $xy$ - $t$  and in the  $k_x k_y$ - $f$  domains, their slowness values being larger than those of the subsurface signals. Aliased energy is especially conspicuous in the  $k_x k_y$ - $f$  domain, wrapping around and obliquely intersecting the true energy. Subsurface signals are also present. Refractions are contained in a conical shape around a smaller two-way time range in the  $xy$ - $t$  domain and inside a conical shape in the  $k_x k_y$ - $f$  domain, which is wider and narrower than for the surface waves. Reflections appear as flat events, i.e., around apices of hyperboloids, with infinitesimally small slowness over the whole two-way time in the  $xy$ - $t$  domain and around the origin  $(k_x, k_y) = (0, 0)$  over all the frequencies in the  $k_x k_y$ - $f$  domain. Figure 1 also depicts  $\vec{N}$  and  $\hat{\vec{P}}$ . The results demonstrate that our method successfully estimates  $\vec{N}$ , even including the aliased energy, and removes it effectively from  $(\vec{P} + \vec{N})$ , providing  $\hat{\vec{P}}$ .

Since our method better handles aliased events, we expect a significant effect on the optimal parameters for survey design.

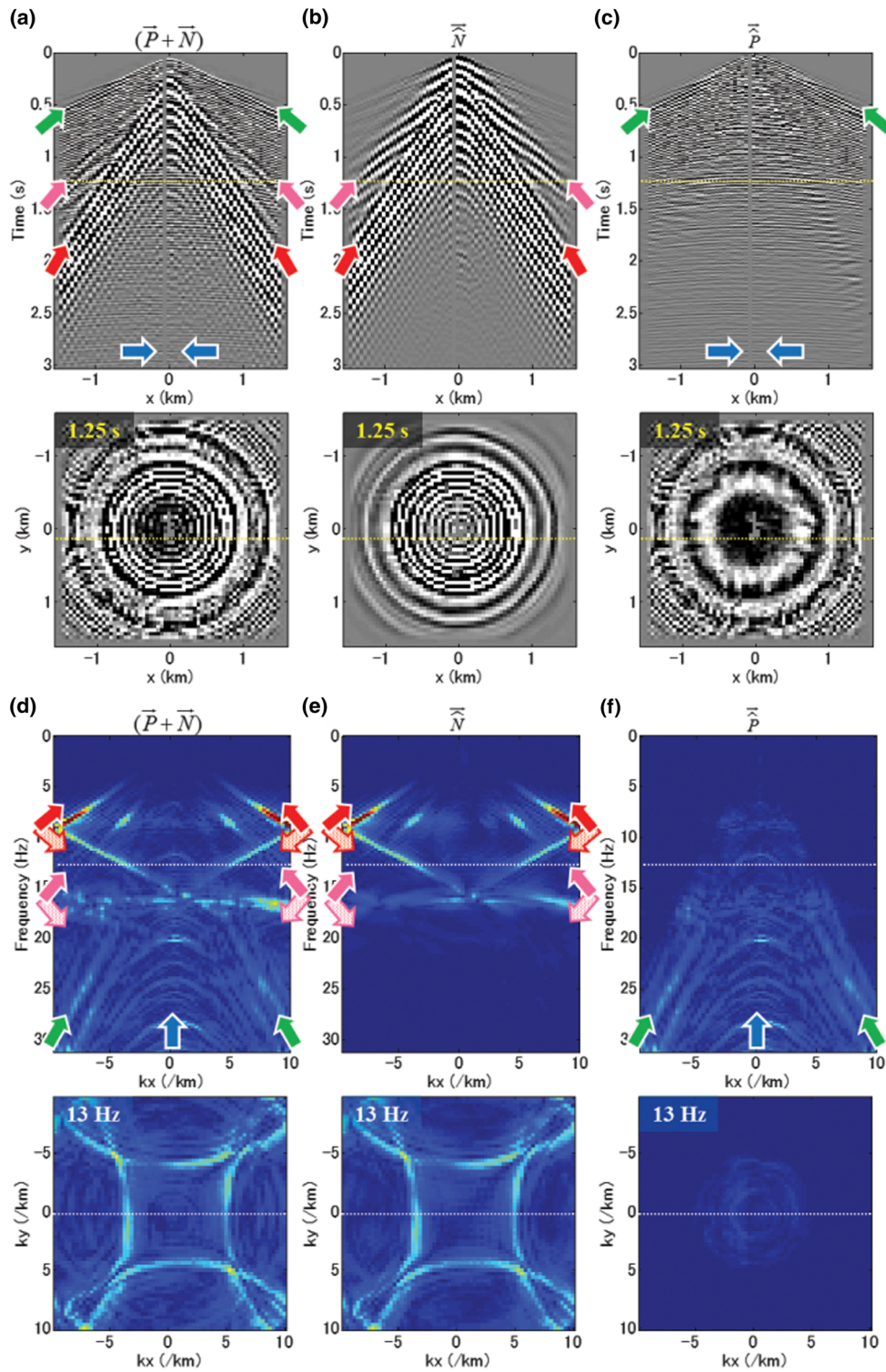


**Figure 1** The results of the surface-wave attenuation using our method (after Ishiyama *et al.* (2015)). (a, d) The seismic data; (b, e) the estimated surface waves; (c, f) the resulting subsurface signals in the  $xy-t$  and the  $k_x k_y - f$  domains with a vertical section at the top and a horizontal time/frequency slice at the bottom. A dotted line in the section indicates the position of the slice, and vice versa. Red, pink, dark green, and blue arrows indicate the surface-wave fundamental mode, a surface-wave higher mode, refractions, and reflections, respectively. A filled arrow indicates the true energy, and the whitish versions of the arrows in the  $k_x k_y - f$  domain indicate the aliased energy of the various wave types. Notice that the surface waves are dispersive, multi-modal, and aliased.

### Data quality

To quantitatively evaluate the data quality resulting from the surface-wave attenuation, we estimate the SNR of  $\tilde{P}$  using the cross-correlation-based method proposed by Thomas, White, and Castoro (1998). After applying a normal-moveout (NMO) correction to  $\tilde{P}$  in the  $xy-t$  domain, reflections correlate from trace to trace. They also correlate with their multiples with a time lag. The surface waves hardly correlate, and their influence can be neglected. Therefore, cross-correlation of traces in a spatial and temporal window that excludes refractions provides an estimate of the subsurface-signal energy,  $E_p$ . Furthermore, if there is a reference data set,  $\tilde{P}_{\text{ref}}$  (for example,  $\tilde{P}$ ), cross-correlation of each trace in  $\tilde{P}$  and the corresponding traces in the spatial/temporal windows in  $\tilde{P}_{\text{ref}}$  improves the estimate,  $E_p$ . Autocorrelation of each trace in  $\tilde{P}$  provides an estimate of the total energy,  $E_{(P+\Delta N)}$ . Therefore, subtracting  $E_p$  from  $E_{(P+\Delta N)}$  provides an estimate of the remaining surface-wave energy,  $E_{\Delta N}$ . Consequently, the SNR is estimated by dividing a representative value of  $E_p$ , such as a spatially summed and averaged value, by that of  $E_{\Delta N}$ . For each monochromatic component, this algorithm can be expressed as

$$(E_{(P+\Delta N)})_{kk} = \hat{P}_k \hat{P}_k^H, \quad (4)$$

$$(E_p)_{kk} = \frac{1}{n_l} \sum_{l=1}^{n_l} \hat{P}_k \hat{P}_{\text{ref}l}^H, \quad (5)$$

$$(E_{\Delta N})_{kk} = (E_{(P+\Delta N)})_{kk} - (E_p)_{kk}, \quad (6)$$

$$\text{SNR} = \frac{\frac{1}{n_d} \sum_{d=1}^{n_d} (E_p)_{dd}}{\frac{1}{n_d} \sum_{d=1}^{n_d} (E_{\Delta N})_{dd}}. \quad (7)$$

$E_{(\cdot)}$  is a diagonal matrix, where both dimensions represent a receiver location. Subscripts  $k, l$ , and  $d$  indicate the receiver location, where  $k$  indicates a location, while  $l$  is used for variable locations in a spatial window centred on the  $k^{\text{th}}$  receiver location, and  $d$  is used for variable locations in the seismic data set. For instance,  $(E_{(\cdot)})_{kk}$  is a non-zero diagonal element of  $E_{(\cdot)}$  and  $\hat{P}_{(\cdot)k}$  is an element of  $\tilde{P}_{(\cdot)}$  for the  $k^{\text{th}}$  receiver location. The numbers  $n_l$  and  $n_d$  are the numbers of receivers in the spatial window and in the seismic data set, respectively. Superscript  $H$  indicates conjugate transposition. To estimate the SNR of the raw data set,  $(\tilde{P} + \tilde{N})$  replaces  $\tilde{P}$  in equations (4) and (5). If there is no reference data set, it is possible to use  $\tilde{P}$  itself for  $\tilde{P}_{\text{ref}}$  in equation (5), although there is no improvement from using  $\tilde{P}_{\text{ref}}$  in this case.

Figures 2 and 3 show an example of the SNR estimation. Figures 2(a)–2(c) exhibit  $(\tilde{P} + \tilde{N})$  and  $\tilde{P}$  after the surface-wave attenuation with our method and with the conventional

one. The latter is a conventional filtering method in the  $k_x k_y - f$  domain. These data sets are the same as used earlier in Fig. 1, followed by NMO correction and trimming to a target temporal window approximately from 1 s to 2 s in the  $xy-t$  domain. Surface waves still lie in a conical shape, reflections are flattened, and multiples are under-corrected. Figure 3 depicts  $E_{(P+\Delta N)}$ ,  $E_{\Delta N}$ , and  $E_p$ , respectively, for these data sets in the  $xy-t$  domain. For  $(\tilde{P} + \tilde{N})$ , surface-wave energy is dominant in a wide range of time lags centred around the zero time lag in the  $xy-t$  domain, with low frequencies around 8 Hz. Energy of reflections is expected to appear at the zero time lag. This subsurface-signal energy peaks around 32 Hz. These various types of energy appear together in  $E_{(P+\Delta N)}$  and separately in  $E_{\Delta N}$  and  $E_p$ . For  $\tilde{P}$ , the results show that the surface-wave energy is well suppressed and the subsurface-signal energy is enhanced after the surface-wave attenuation. Figure 2(d) displays the energy spectra of these data sets. To generate these spectra, we averaged  $E_{\Delta N}$  and  $E_p$  over the space in the  $xy-f$  domain. The surface-wave spectrum mainly contains surface-wave energy up to around 30 Hz. Above this frequency, it possibly also contains some unexplained noise. The results again show that the surface-wave energy is well suppressed in the dominant frequencies. The SNR is consequently improved, i.e., the residual surface-wave spectrum has less energy.

If these spectra are averaged over a frequency window from 2 Hz to 50 Hz, the resulting SNR is 0.02 (−32 dB) for  $(\tilde{P} + \tilde{N})$ , 0.77 (−2 dB) for  $\tilde{P}$  after the surface-wave attenuation using our method, and 0.32 (−10 dB) using the conventional one. Our method improves a better SNR than the conventional one, although some residual surface-wave energy still remains, visible as peaks around 8 Hz and 16 Hz.

### A CASE STUDY

We applied the surface-wave attenuation and the SNR estimation to several data sets obtained by decimating 3-D OBC hydrophone data, originally acquired in a shallow-water environment offshore Abu Dhabi. Table 1 lists the basic subsets. The abbreviation “BS” means “basic subset”. This is followed by a number, related to the survey effort in ascending order, and by a single character, where “a” denotes “symmetric”, i.e.,  $A_{\Delta x_b} = 1$  and  $A_{X_b} = 1$ ; “b” marks “asymmetric” in terms of the spatial sampling intervals, i.e.,  $A_{\Delta x_b} \neq 1$ ; and “c” indicates that the spatial sampling apertures are larger than those of the reference basic subset, i.e.,  $X_b > X_{b\text{ref}}$  and/or  $Y_b > Y_{b\text{ref}}$ . The  $x$ -direction corresponds to the in-line direction. For the survey effort, we chose

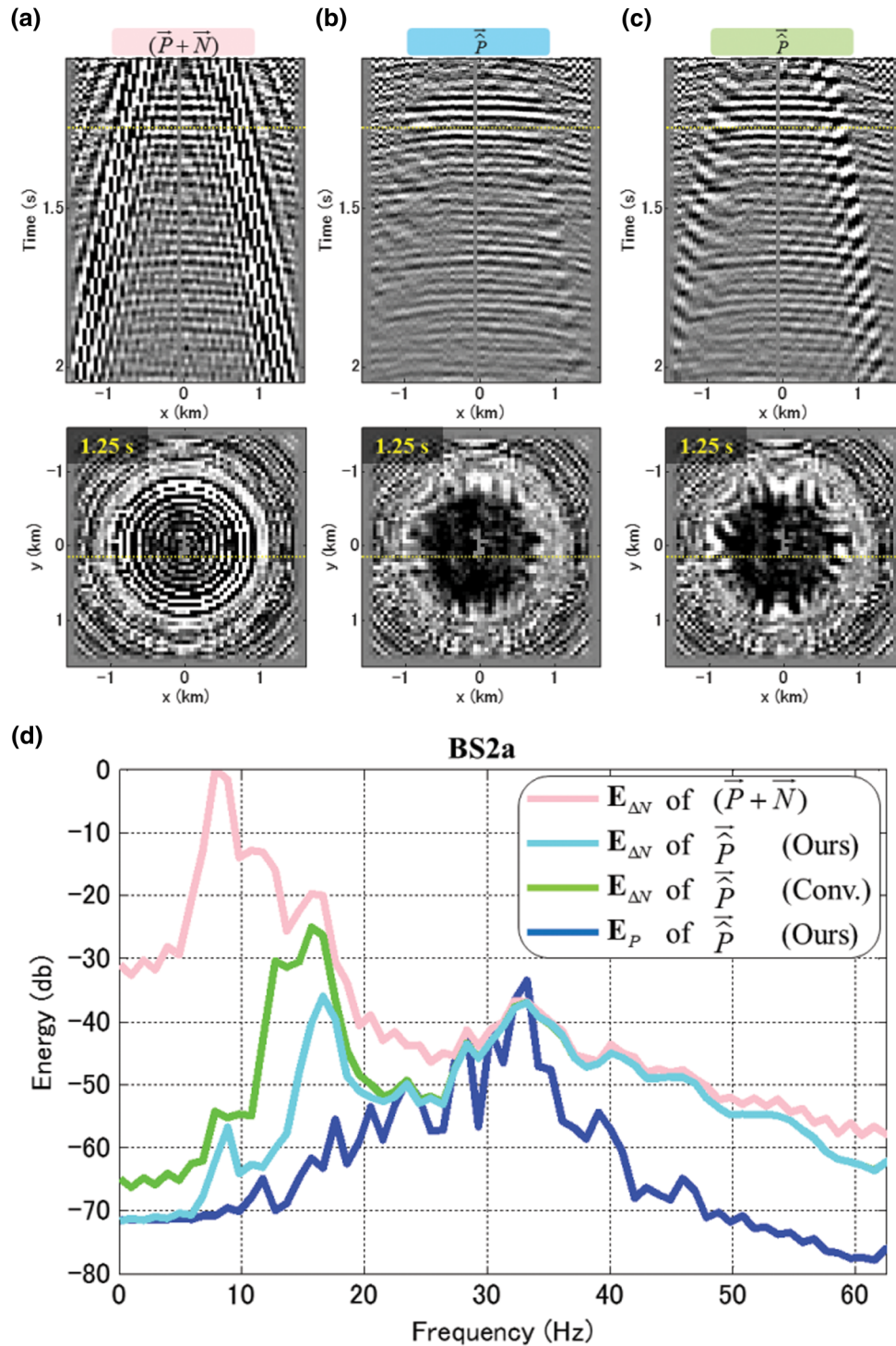


Figure 2 The energy spectra for a basic subset (BS2a). (a) The raw data set; (b, c) the subsurface-signal data sets after the surface-wave attenuation using our method, and the conventional one, with a vertical section at the top and a horizontal time slice at the bottom. A dotted line in the section indicates the position of the slice, and vice versa. (d) The energy spectra. The magenta, cyan, and green lines indicate the surface-wave energy of the data sets (a), (b), and (c), respectively. The blue line marks the subsurface-signal energy of the data set (b). If the spectra are averaged over a frequency window between 2 Hz and 50 Hz, the resulting SNR is 0.02 (−32 dB) for  $(\bar{P} + \bar{N})$ , 0.77 (−2 dB) for  $\bar{P}$  after the surface-wave attenuation using our method, and 0.32 (−10 dB) using the conventional one.

**Figure 3** The energy estimates for a basic subset (BS2a). Those of the raw data set (a1–c1), the subsurface-signal data sets after the surface-wave attenuation using our method (a2–c2), and the conventional one (a3–c3). (a) The total energy; (b) the surface-wave energy; (c) the subsurface-signal energy, with a vertical section at the top and a temporary-summed and averaged slice at the bottom. A dotted line in the slice indicates the position of the section.

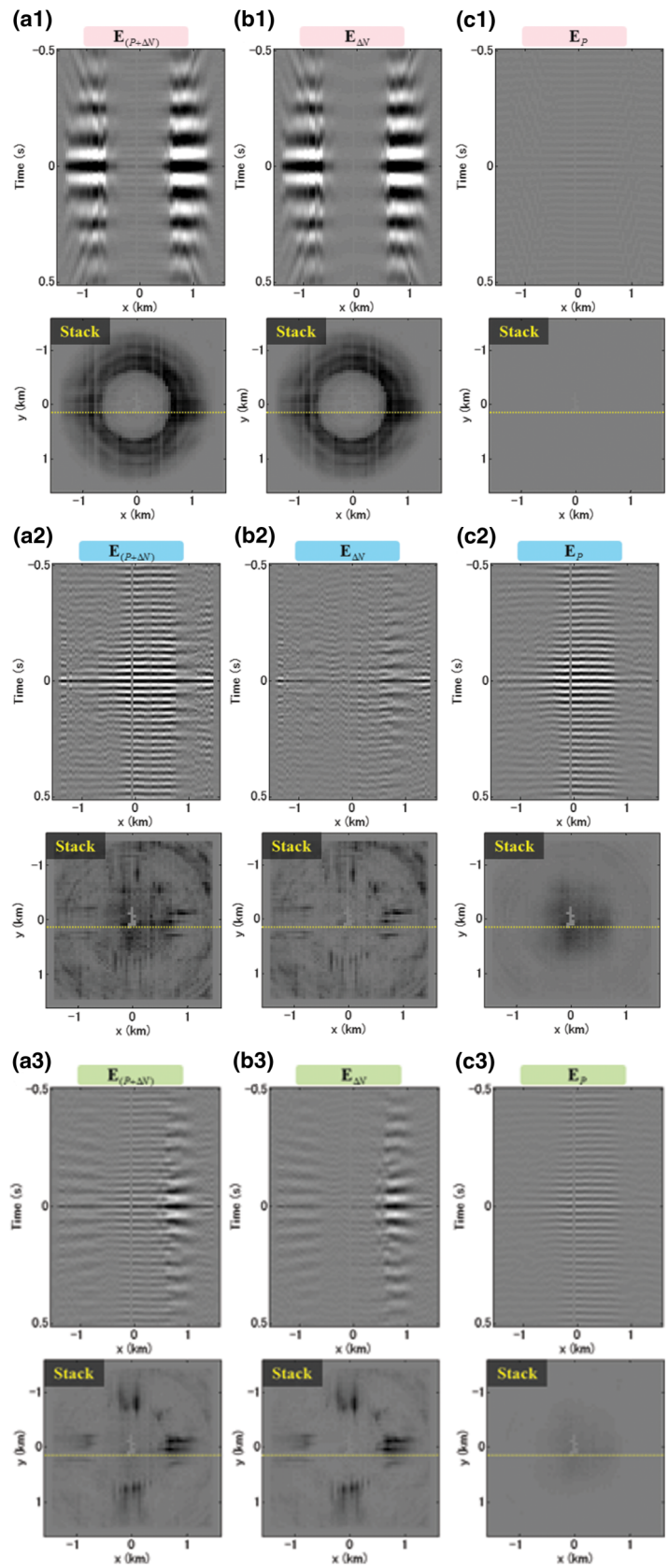


Table 1 List of the basic subsets

Geometry	$\Delta x_b$ (m)	$\Delta y_b$ (m)	$X_b$ (m)	$Y_b$ (m)	$A_{\Delta x_b}$	$A_{X_b}$	SE
BS1a	100	100	3200	3200	1.00	1.00	0.0625
BS2a	50	50	3200	3200	1.00	1.00	0.25
BS2b	25	100	3200	3200	0.25	1.00	0.25
BS3b	25	50	3200	3200	0.50	1.00	0.50
BS3c	50	50	6400	3200	1.00	0.50	0.50
BS4a	25	25	3200	3200	1.00	1.00	1.00
BS4c	50	50	6400	6400	1.00	1.00	1.00

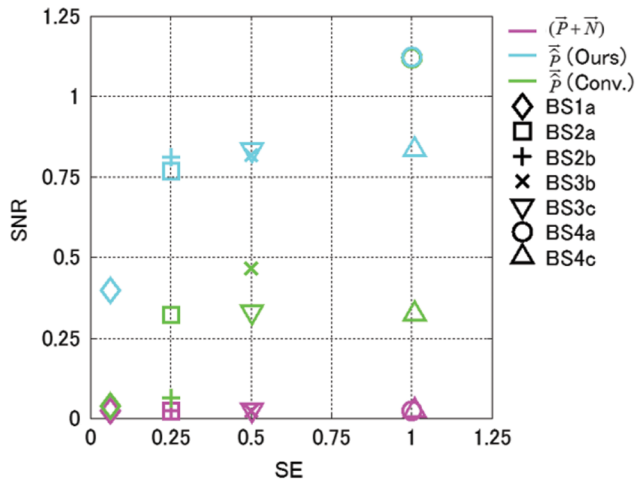


Figure 4 SNR as a function of SE for the data sets in Table 1. Magenta symbols correspond to the raw data sets, cyan symbols correspond to the subsurface-signal data sets after the surface-wave attenuation using our method, and green symbols using the conventional one.

a reference basic subset with  $\{\Delta x_{bref}, \Delta y_{bref}, X_{bref}, Y_{bref}\} = \{25 \text{ m}, 25 \text{ m}, 3200 \text{ m}, 3200 \text{ m}\}$  denoted by BS4a. We took the result after surface-wave attenuation with our method as a reference data set for the SNR estimation. To allow for a fair comparison of the results, the same processing parameters of the surface-wave attenuation and the same velocity for NMO correction were applied to all data sets whenever possible. The SNR was estimated in the same area of interest, with the same spatial, temporal, and frequency windows as used earlier in Figs. 2 and 3, for all data sets.

Figure 4 shows the SNR as a function of the survey effort, SE. The horizontal axis is for SE, and the vertical axis is for SNR. The magenta samples mark the values for the raw data set,  $(\bar{P} + \bar{N})$ . The subsurface-signal data set,  $\hat{P}$ , after the surface-wave attenuation using our method is coloured cyan, whereas the results after the conventional one are coloured

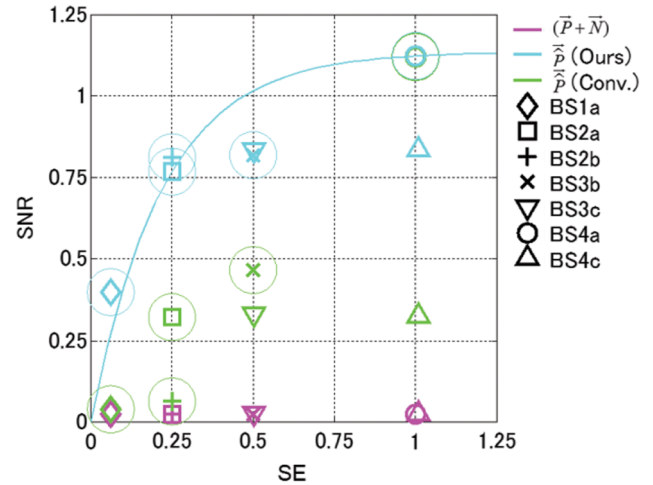
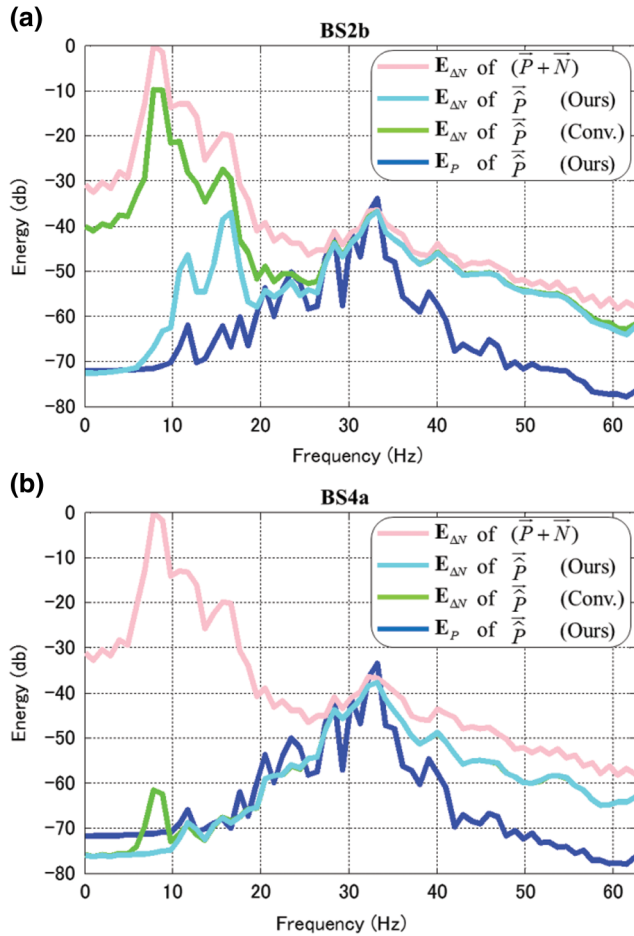


Figure 5 As Fig. 4, but now the outer circles highlight samples with finer spatial sampling intervals. The cyan line represents a curve obtained by fitting these cyan samples to the equation  $SNR(SE, \beta) = \alpha[1 - e^{-\beta(A_{\Delta x_b})^{SE}}]$ , where  $\alpha$  is a constant and  $\beta$  generally depends on  $A_{\Delta x_b}$ . In this example,  $\alpha = 1.14$  and  $\beta = 4.52$ , assuming that  $\beta$  is a constant.

green. For the magenta samples, the SNR is consistently very low due to the dominance of the surface-wave energy. In general, the cyan samples fall in the upper left, and the green samples fall in the lower right, showing that our method provides a better SNR than the conventional one.

### Effects of spatial sampling intervals

If we decrease the spatial sampling intervals or increase the spatial sampling apertures, the SNR should generally improve, but the price paid is a larger survey effort. Samples highlighted by an outer circle in Fig. 5 correspond to cases with finer spatial sampling intervals. For these samples, the SNR increases with SE. Figures 2(d), 6(a), and 6(b) show the energy spectra for some of these cases, namely, BS2a, BS2b, and BS4a. For BS2a and BS2b, the surface-wave energy is well suppressed and the SNR is consequently improved by the surface-wave attenuation. Our method clearly provides a better SNR than the conventional one. However, for BS4a, the SNR is improved to the same level for both methods. This is because BS4a has spatial sampling intervals that are sufficiently fine to avoid aliased surface-wave energy. This aliased energy is a main cause of residual surface-wave energy after the surface-wave attenuation. Therefore, for data sets that do not contain aliased energy, the resulting SNR does not depend so much on the choice of method. In this case, a further decrease in the spatial sampling intervals will generally not help to further



**Figure 6** The energy spectra for (a) BS2b and (b) BS4a. The magenta, cyan, and green lines indicate the surface-wave energy of the raw data sets, the subsurface-signal data sets after the surface-wave attenuation using our method, and the conventional one, respectively. The blue line marks the subsurface-signal energy of the second data set. As for (a) BS2b, the resulting SNR is 0.02 (−33 dB) for  $(\bar{P} + \bar{N})$ , 0.81 (−2 dB) for  $\bar{P}$  after the surface-wave attenuation using our method, and 0.06 (−24 dB) using the conventional one. For (b) BS4a, the resulting SNR is 0.02 (−32 dB) for  $(\bar{P} + \bar{N})$ , 1.12 (+1 dB) for  $\bar{P}$  after the surface-wave attenuation using our method, and 1.12 (+1 dB) using the conventional one.

improve the SNR. The spatial sampling intervals are the key types of survey parameters. Decreasing the spatial sampling intervals improves the resulting data quality until a plateau is reached where surface-wave energy is no longer aliased and can be easily removed. To emphasize this, in Fig. 5, we fitted an *ad hoc* curve to the cyan samples obtained with our method. It illustrates the main trend of the relationship between the spatial sampling intervals and the the resulting data

quality. Obviously, the method of surface-wave attenuation determines its shape.

### Effects of the symmetry

As far as symmetry of the spatial sampling intervals is concerned, BS2a and BS4a are symmetric with  $A_{\Delta x_b} = 1$ , whereas BS2b with  $A_{\Delta x_b} = 0.25$  is not. For the cyan samples with our method in Fig. 5, the SNR of BS2b is slightly better than that of BS2a at the same SE. For BS2b, as compared with BS2a, the remaining surface-wave energy  $E_{\Delta N}$  is suppressed better in the  $x$ -direction and fairly well in the  $y$ -direction. This is because BS2b has a finer spatial sampling interval in the  $x$ -direction. However, in terms of the spatial distribution,  $E_{\Delta N}$  is still present in the  $y$ -direction, particularly around the near  $x$ -offsets, whereas in the symmetric case of BS2a, it is shared equally between both horizontal directions. The degree of asymmetry in the spatial sampling intervals affects the spatial distribution of the pre-stack SNR. This is not the case, however, for the green samples, obtained with the conventional method, that correspond to BS2a and BS2b in Fig. 5. The SNR of BS2a is better than that of BS2b at the same SE. This is because, for BS2b, the surface-wave energy is suppressed very poorly in the  $y$ -direction, though well enough in the  $x$ -direction. In summary, we see that the degree of asymmetry may provide a better or a worse SNR and we cannot draw a general conclusion.

### Effects of spatial sampling apertures and the symmetry

Samples highlighted by an outer circle in Fig. 7 correspond to cases where the larger spatial sampling apertures increase the survey effort. For these samples, the SNR hardly changes with SE. Figures 2(d), 8(a), and 8(b) show the energy spectra for these samples, BS2a, BS3c, and BS4c. In all cases, the attenuation of the surface-wave energy is similar and the SNR is improved to the same level by the surface-wave attenuation. This tendency is observed both for our method and the conventional one. In summary, extending the spatial sampling apertures does not contribute to increasing the resulting data quality in terms of the surface-wave attenuation. Therefore, the symmetry of the spatial sampling apertures does not matter either.

### Discussion

The results of this case study show that the spatial sampling intervals are the essential types of survey parameters in terms

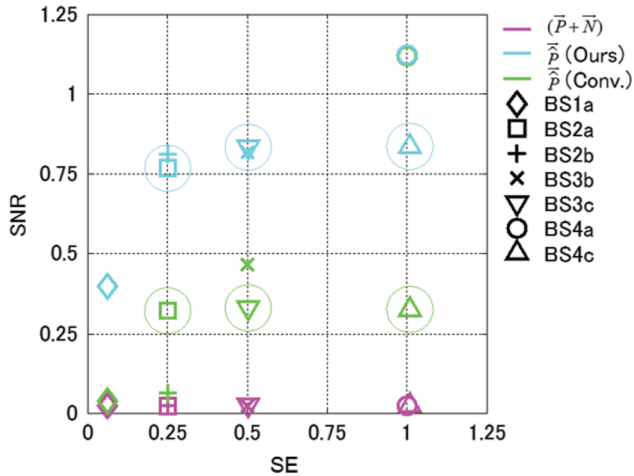


Figure 7 As Fig. 4, but now the outer circles highlight samples with larger sampling apertures.

of surface-wave attenuation. Finer spatial sampling intervals improve the resulting data quality until a plateau is reached. This is the main trend of the relationship between the spatial sampling intervals and the resulting data quality. Given a required data quality, optimal values of the spatial sampling intervals can be found on the main trend curve. The resulting data quality is also related to the method of surface-wave attenuation. For instance, our method works even for aliased surface waves, whereas the conventional one does not. Some other methods may work even better, e.g., by handling scattered surface waves. Therefore, the shape of the main trend curve depends on the method of surface-wave attenuation. This means that a proper choice of the methods offers the possibility of relaxing the spatial sampling intervals and, therefore, should be taken into account in survey design. For instance, one can see in Fig. 5 at which values of the spatial sampling intervals the required data quality is achieved or exceeded. If the required pre-stack SNR is 0.75, the survey effort in terms of the spatial sampling intervals could be 0.25 when using our method, whereas the effort should be higher, close to 1.0, when using the conventional method. This is important in survey design because we seek survey parameters to achieve sufficient data quality at the least survey effort.

Seismic data naturally vary field by field due to the different subsurface/near-surface structures/properties. Therefore, the shape of the above main trend curve is not universal. It may not be practical to acquire a pilot seismic survey in a field just to obtain the main trend. However, it is possible to use an existing real data set from a nearby or similar area that contains typical seismic events for the region. Then,

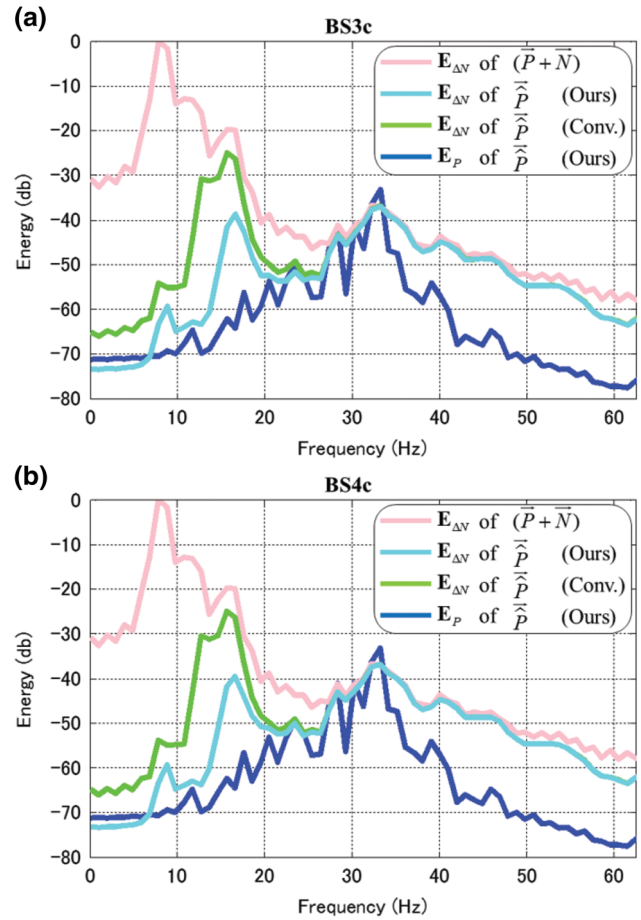


Figure 8 The energy spectra for (a) BS3c and (b) BS4c. The magenta, cyan, and green lines indicate the surface-wave energy of the raw data sets, the subsurface-signal data sets after the surface-wave attenuation using our method, and the conventional one, respectively. The blue line marks the subsurface-signal energy of the second data set. As for (a) BS3c, the resulting SNR is 0.02 (−32 dB) for  $(\bar{P} + \bar{N})$ , 0.83 (−2 dB) for  $\hat{P}$  after the surface-wave attenuation using our method, and 0.33 (−10 dB) using the conventional one. For (b) BS4c, the resulting SNR is 0.02 (−32 dB) for  $(\bar{P} + \bar{N})$ , 0.84 (−2 dB) for  $\hat{P}$  after the surface-wave attenuation using our method, and 0.33 (−10 dB) using the conventional one.

we can obtain several data sets by decimating the original and carry out the same study to understand the main trend in data quality as a function of survey effort. Alternatively, we can generate a synthetic data set, e.g., simulated by a 3-D elastic finite-difference code, particularly if there is no real data set in which the spatial sampling intervals are not sufficiently fine to be subsequently decimated. However, this may introduce more uncertainty in the main trend because the accuracy of the trend curve depends on the realism of the

subsurface/near-surface models used in the simulation. Nevertheless, the trend curve can be still used if it is calibrated with one derived from existing real data at coarse spatial sampling intervals.

The results of this case study also show that the degree of asymmetry in the spatial sampling intervals affects the spatial distribution of the pre-stack SNR in the basic subset. The pre-stack SNR is improved relatively more in the direction of finer sampling. Given a required data quality, either for post-stack applications or pre-stack applications such as pre-stack imaging and amplitude-versus-offset-and-azimuth (AVOAz) analysis, optimal values of the aspect ratio can be considered. Therefore, again, survey design should take processing steps into account, as well as the requirements for reservoir characterization. Feedback from data processors and interpreters to survey designers is vital in this regard.

## CONCLUSIONS

We have analysed the relationship between the survey parameters and the resulting data quality in the context of surface-wave attenuation. The impact of the acquisition geometry on the effectiveness of surface-wave attenuation can be summarized as follows.

- The spatial sampling intervals of the basic subset are the key types of survey parameters. Finer spatial sampling intervals improve the resulting data quality until it levels off when the surface waves are no longer aliased and can be easily removed.
- A degree of asymmetry in the spatial sampling intervals affects the spatial distribution of the pre-stack data quality in the basic subset. The pre-stack data quality is improved mainly in the direction of finer sampling.
- Larger spatial sampling apertures do not contribute to a better data quality. The symmetry of the spatial sampling apertures does not matter either.
- The method of surface-wave attenuation affects the resulting data quality. Our method produces a much better data quality at a given survey effort than conventional filtering methods. Alternatively, a similar data quality can be reached at considerably lower cost.

## ACKNOWLEDGEMENTS

The authors would like to thank Adnoc and their R&D Oil Sub-Committee for their permission to use the data from offshore Abu Dhabi and publish this paper. The authors acknowledge Inpex for their financial support for this research. The authors are grateful to the Delphi Consortium sponsors for their support and discussions on this subject. They would also like to thank the anonymous reviewers for their constructive comments.

## REFERENCES

- Berkhout A.J. 1982. *Seismic Migration: Imaging of Acoustic Energy by Wavefield Extrapolation, Part A: Theoretical Aspects*. Elsevier.
- Berkhout A.J., Ongkiehong L., Volker A.W.F. and Blacquièrè G. 2001. Comprehensive assessment of seismic acquisition geometries by focal beams – Part I: Theoretical considerations. *Geophysics* **66**, 911–917.
- Berteussen K., Zhang Z. and Sun Y. 2011. Surface wave analysis of Arabian Gulf ocean bottom seismic data. 73rd EAGE Conference and Exhibition, Extended Abstracts.
- Cordson A., Galbraith M. and Peirce J. 2000. *Planning Land 3-D Seismic Surveys*. Society of Exploration Geophysicists.
- Galbraith M. 2004. A new methodology for 3D survey design. *The Leading Edge* **23**(10), 1017–1023.
- Ishiyama T. and Blacquièrè G. 2015. 3-D shallow-water seismic survey design and evaluation using the focal-beam method: A case study offshore Abu Dhabi. *Geophysical Prospecting*, Accepted and published online.
- Ishiyama T., Blacquièrè G., Verschuur D.J. and Mulder W.A. 2015. 3-D surface-wave estimation and separation using a closed-loop approach. *Geophysical Prospecting*, Accepted and published online.
- Thomas R., White R. and Castoro A. 1998. Quantitative controls on 3-D seismic processing for prestack attribute analysis. *The Leading Edge* **17**(11), 1596–1599.
- van Veldhuizen E.J., Blacquièrè G. and Berkhout A.J. 2008. Acquisition geometry analysis in complex 3D media. *Geophysics* **73**, Q43–Q58.
- Vermeer G.J.O. 2012. *3-D Seismic Survey Design*. Society of Exploration Geophysicists.
- Volker A.W.F., Blacquièrè G., Berkhout A.J. and Ongkiehong L. 2001. Comprehensive assessment of seismic acquisition geometries by focal beams – Part II: Practical aspects and examples. *Geophysics* **66**, 918–931.
- Yilmaz O. 2001. *Seismic Data Analysis*. Society of Exploration Geophysicists.